# As-Cast Residual Stresses in an Aluminum Alloy AA6063 Billet: Neutron Diffraction Measurements and Finite Element Modeling

J.-M. DREZET and A.B. PHILLION

The presence of thermally induced residual stresses, created during the industrial direct chill (DC) casting process of aluminum alloys, can cause both significant safety concerns and the formation of defects during downstream processing. Although numerical models have been previously developed to compute these residual stresses, most of the computations have been validated only against measured surface distortions. Recently, the variation in residual elastic strains in the steady-state regime of casting has been measured as a function of radial position using neutron diffraction (ND) in an AA6063 grain-refined cylindrical billet. In the present study, these measurements are used to show that a well-designed thermomechanical finite element (FE) process model can reproduce relatively well the experimental results. A sensitivity analysis is then carried out to determine the relative effect of the various mechanical parameters when computing the as-cast residual stresses in a cylindrical billet. Two model parameters have been investigated: the temperature when the alloy starts to thermally contract and the plasticity behavior. It is shown that the mechanical properties at low temperatures have a much larger influence on the residual stresses than those at high temperatures.

DOI: 10.1007/s11661-010-0424-y

## I. INTRODUCTION

THE fabrication of aluminum alloy extrusion products typically involves a number of steps starting from the semicontinuous casting of the cylindrical billet using a process known as direct chill (DC) casting and, depending on the alloy composition, ending with a postextrusion heat treatment. Of the different processing stages, the casting process is particularly violent since it gives rise to large thermally induced strains that can result in several types of casting defects including distortions, cracks, porosity, *etc*. Although these thermally induced strains can be partially relieved by permanent deformation, cracks will be generated either during solidification (hot tears) or postsolidification cooling (cold cracks) when the corresponding stresses exceed the deformation limit of the alloy.[1] Furthermore, the thermally induced strains generally result in the development of large residual stresses within the billet upon cooling. These residual stresses will cause significant downstream processing and safety issues during the sawing stage prior to extrusion, when the billet is cut into section of about 1 m in length. For large diameter (typically greater than 350 mm) and high-strength alloys (2xxx and 7xxx series), the residual stresses can lead to saw pinching or crack initiation. In both cases, the elastic energy released upon sawing may cause personnel injury and equipment damage.

Currently, the most common technique for quantifying residual stresses that arise during manufacturing is through the use of numerical process models, generally using finite element (FE) computational techniques. To be effective and accurate, these models require a significant understanding of the processing route and knowledge of the material's mechanical and physical behavior over a range of temperatures. The computation of stress evolution including billet distortions and residual stresses during the DC casting of aluminum alloys has been the scope of many studies since the late 1990s[2] and nowadays is a well-established technique. However, validation of these models, often done by comparing the computed and measured distortions at the billet surface, *e.g.*, the butt-curl[8] and the rolling face pull-in for rolling sheet ingots,[9] remains challenging. Experimental validation against the computed room-temperature residual stresses is limited simply owing to the difficulty of measuring the internal strains in large castings and the high variability in the measurements. While some measurement techniques are available for quenching[11] or welding,[12] they remain rare, uncertain, and are usually limited to only one or two components of the stress tensor near the surface of the casting.[5,13] In the past, destructive methods (hole drilling,[14] cut compliance,[15] *etc*.) have been used for measuring residual elastic strains. Physical methods such as X-ray, ultrasound, or neutron diffraction (ND) have now become very attractive,[16,17] since they can provide

---

J.-M. DREZET, Senior Scientist, is with LSMX, Ecole Polytechnique Fédérale de Lausanne, Station 12, CH-1015 Lausanne, Switzerland. Contact e-mail: jean-marie.drezet@epfl.ch A.B. PHILLION, Assistant Professor, is with the School of Engineering, University of British Columbia, Kelowna, BC V1V 1V7, Canada.
Manuscript submitted June 8, 2010.

all of the components of the elastic deformation tensor. These physical methods also now allow for measurement deep within a sample up to the energy limit of the beam. With the development of powerful neutron beams, it is now possible to measure the residual elastic strains rather deep in light metal alloy systems such as aluminum and magnesium alloys.[18] Such measurement allows for sophisticated model validation.

Recently, in order to validate the simulation methodology previously developed by the authors[2,7,10] to model the thermal and stress/strain evolution during the DC casting process of aluminum alloys, the residual elastic strains in a grain-refined AA6063 billet were measured using ND.[19] In the present study, these ND measurements together with a FE model of the DC casting process have been used to investigate the effects of the input mechanical and physical properties on the magnitude and distribution of the residual stress predictions. First, the principles of residual elastic strain measurement using ND are recalled together with the equations for converting strains into stresses. Issues such as the beam paths and billet positioning are also detailed. Second, the FE model used to compute the residual stresses after the casting process is presented along with the mechanical and physical properties of the AA6063 alloy. Third, the residual elastic strains and stresses predicted by the FE model are presented and compared to the ND measurements. Finally, the results of the sensitivity analysis conducted on the alloy's material properties are provided and discussed.

## II. ND MEASUREMENTS

The methodology used to measure the residual elastic strains in a DC cast billet and the corresponding stress calculations are built on the experimental aspects presented in a prior publication[19] and presented in Sections II–A and II–B.

### A. *Principles of Strain Measurement via ND*

The residual elastic strain measurements were conducted using the POLDI apparatus[20,21] of the Swiss Spallation Neutron Source SINQ, Paul Scherrer Institut (Villigen, Switzerland), through accurate determination of the lattice spacings. These lattice spacings can be derived through application of Bragg's law, $\lambda = 2d \sin \theta$, where $d$ is the lattice spacing, $\lambda$ the wavelength, and $2\theta$ the diffraction angle. POLDI is a so-called time-of-flight instrument; the detector is placed at a fixed 90 deg angle and the billet bombarded by neutrons. With this configuration, the lattice spacings are then calculated from the wavelength of the diffracted neutrons captured by the detector. The position of the diffraction peak is a measure of the average lattice spacing, while the width of the data is related to the fluctuations in the crystal structure. The measured lattice spacing acts as a strain gage in combination with a stress-free lattice spacing $d_0$:

$$\varepsilon_{el} = \frac{d - d_0}{d_0} \qquad [1]$$

### B. *Experimental Methodology*

To investigate the residual stresses during the aluminum casting process, a round billet of type AA6063 was DC cast at the Alcan ATI Valais industrial casting facility. This grain-refined billet of 160-mm radius with a grain size of $100 \pm 30\ \mu$m, no grain texture, and composition (wt pct) Al-0.52Si-0.18Fe-0.013Zn-0.09 Cu-0.60Mg-0.07Mn-0.013Cr was cast at 66 mm/min.

In order to measure the residual elastic strains in the aluminum AA6063 billet using POLDI, the cast billet was cut to a length of 480 mm. As shown previously,[19] this sawing activity will not relax the residual stresses midheight in the section as long as the billet section length is greater than 3 times the billet radius. This central portion of the billet was then placed within the POLDI device to acquire the stressed lattice spacings along the billet radius in each direction. Although the generalized elastic strain tensor contains six components, the DC casting process of a round billet is axisymmetric in geometry and in the casting conditions, reducing this tensor to four components. Furthermore, since the billet section of interest was taken from the central part or steady-state regime of the casting, it can be assumed that the elastic strains vary only as a function of radial position. In addition, it was shown with the help of the FE model of DC casting that the shear stress ($rz$) component is negligible,[19] and thus only the radial, hoop, and axial strain and stress components are nonzero.[4] The elastic deformation tensor corresponding to this scenario will be diagonal in the ($r$, $\theta$, $z$) reference frame. As such, the residual elastic strains can be converted to residual stresses using Hooke's law, where $E = 71.3$ GPa is Young's modulus and $v = 0.3$ the Poisson's ratio:

$$\sigma = \begin{pmatrix} \sigma_r \\ \sigma_\theta \\ \sigma_z \end{pmatrix} = \frac{E}{(1+v)(1-2v)} \begin{pmatrix} 1-v & v & v \\ v & 1-v & v \\ v & v & 1-v \end{pmatrix} \begin{pmatrix} \varepsilon_r \\ \varepsilon_\theta \\ \varepsilon_z \end{pmatrix} \qquad [2]$$

To calculate the variation in residual elastic strains within the billet, the stressed lattice spacings, $d$, were measured in the radial, hoop, and axial directions using ND along the billet radius approximately every 20 mm. In total, 22 measurements were made, with one measurement corresponding to one strain component at one position, on a sample gage volume of $3.8 \times 3.8 \times 8\ \text{mm}^3$. Although this volume is rather large, the 3.8-mm collimator was used to ensure a high neutron transmission of ~78 pct and, correspondingly, a reasonable measurement time, typically 2 hours per measurement and 400,000 counts. In order to acquire the lattice spacings for each of the three measured strain components, both the beam orientation and the position of the billet within the neutron chamber were varied, as shown in Figure 1. For the radial component, the length of the beam path varied from almost zero at the billet surface

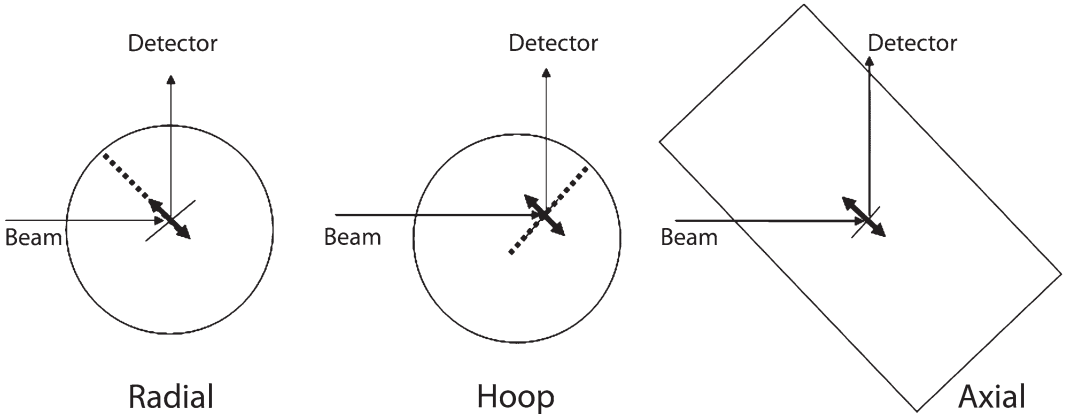

Fig. 1—Configuration and associated beam pathway for radial (left), hoop (centre) and axial (right) strain measurements. Thin lines represent the direction of the diffracting planes whereas double arrows represent the direction of the strain components.

to $2R$ at the billet center. For the hoop component, the beam path remained near $2R$ for each measurement, whereas for the axial component, the beam path increased from almost zero at the billet surface to $2\sqrt{2}RR$ at the billet center. The stress-free lattice constant ($d_0$) was also measured using ND on small samples, 3 mm in height and 2 mm in diameter, that had been electrodischarge machined every 20 mm along the billet radius. These measurements indicated that $d_0$ was not influenced by compositional variations along the billet radius and was very close to the standard lattice constant for aluminum, 4.0504 Å. The measured lattice spacings, $d$, were then converted to strains using $d_0$ and Eq. [1].

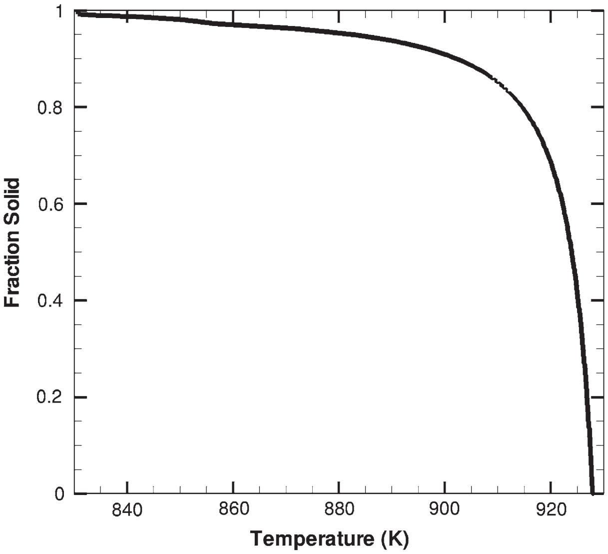

Fig. 2—Evolution in volume fraction solid with temperature for the AA6063 alloy.[23]

## III. THERMOMECHANICAL FE MODEL

The DC casting process of an AA6063 aluminum round billet was simulated using an axisymmetric coupled thermomechanical model implemented in the commercial FE code ABAQUS* 6.8.

### A. *FE Model of DC Casting*

The computational domain includes both the start-up and steady-state regions of the billet. The mesh consists of 100 layers of elements, each with an 11-mm-high layer containing 19 elements, for a total cast length of 1100 mm. Due to symmetry, only one-half of the round billet was modeled. In order to simulate the casting process, the coordinate system was fixed with respect to the billet, and the incoming flow of liquid metal was modeled through the activation of successive layers at a rate that corresponds to the experimental casting speed of 66 mm/min. The total simulation time was 4600 seconds: 10 seconds per added layer plus a 3600-second cool down period. The initial condition was a pouring temperature of 943 K (670 °C). The horizontal boundary conditions were also moved up along the domain at a rate of 66 mm/min. These boundary conditions account for primary cooling through the mold, air gap formation, and secondary cooling at the point where the water hits the billet and flows along its surface. Further details on these boundary conditions can be found in Reference 22.

### B. *Thermophysical Properties*

The temperature-dependent thermophysical properties of the AA6063 alloy (heat capacity, latent heat, and thermal conductivity) measured by Doré *et al.*,[23] along with the Young's modulus and the coefficient of thermal expansion (CTE) measured as part of the European project EMPACT,[24,25] were used in the current study. The Poisson's ratio was assumed to be 0.3. The solidification path of the alloy, shown in Figure 2, was also taken from the work of Doré[23] assuming a solidification time of 104 seconds. The liquidus and

---

*ABAQUS is a trademark of Dassault Systems Inc., Providence, RI.

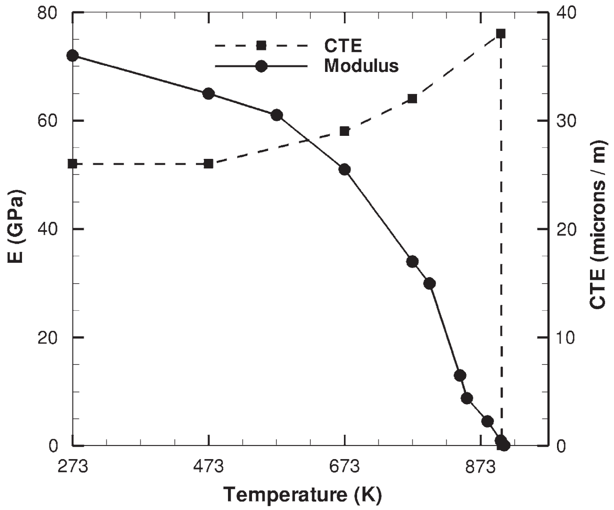

Fig. 3—Young's modulus (left scale) and CTE (right scale) *vs* temperature for the AA6063 alloy.[24,25]

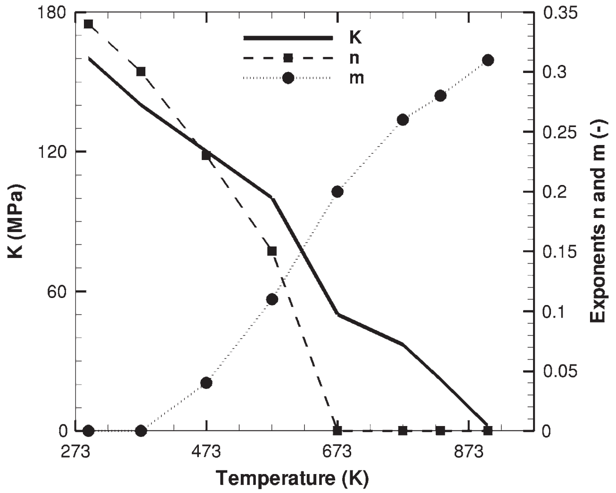

Fig. 4—Temperature variation of the consistency, *K*, and exponents, *n* and *m*, for the AA6063 alloy in the as-cast state.[24,25]

solidus temperatures were 928 K and 830 K (655 °C and 557 °C), respectively.

To properly simulate the DC casting process using FEs, the thermophysical properties need to include the change in behavior that occurs during solidification, specifically, the effect of solidification on rheology, and the corresponding increase in Young's modulus and CTE that occur with increasing fraction solid. The fraction solid at which the alloy starts to exhibit solid thermal contraction is generally considered to be close to the fraction solid for mechanical coalescence,[26] *i.e.*, the point at which the solidifying material is able to develop stress. Based on the work by Doré,[23] the thermal contraction for AA6063 starts at $T_{\mathrm{coal}} = 903$ K (630 °C) in AA6063 and corresponds to a fraction solid, $f_{s,\mathrm{coal}} = 0.88$. In AA6061, an alloy that has a composition close to the alloy retained in the present study, Strangeland *et al.*[27] reported similar values, between 0.85 and 0.92, for the fraction solid at the onset of thermal contraction. In the model, the CTE at temperatures above $T_{\mathrm{coal}}$ was assumed to be zero, and the Young's modulus was decreased as follows: from 10 GPa at $T_{\mathrm{solidus}}$ to 0.1 GPa at $T_{\mathrm{coal}}$ and to 0.01 GPa at $T_{\mathrm{coal}} + 5$ K. This variation in modulus and CTE was implemented in an attempt to ensure a low level of stress in the metal above $T_{\mathrm{coal}}$ while avoiding convergence issues. The variation of these two properties as a function of temperature between the liquidus and room temperature is shown in Figure 3.

### C. *Mechanical Behavior*

The mechanical behavior of the AA6063 alloy was modeled as an elasto-viscoplastic material with a yield stress that increases with decreasing temperature below $T_{\mathrm{coal}}$. The effects of strain and strain rate on stress formation, *i.e.*, strain hardening and strain-rate dependence, were also taken into account. The constitutive equation governing this mechanical behavior can be approximated using a modified form of Ludwik's equation:[7,28,29]

$$\bar{\sigma} = K(T)\varepsilon_p^{n(T)}\left(\frac{\dot{\varepsilon}_p}{\dot{\varepsilon}_0}\right)^{m(T)} \qquad [3]$$

where $\bar{\sigma}$ is the von Mises equivalent stress, $\dot{\varepsilon}_p$ is the equivalent inelastic strain rate, and $\dot{\varepsilon}_0$ is a constant taken as 1 $\mathrm{s}^{-1}$. The modified Ludwik equation was used since it is well suited to describe the transition from time-independent plasticity at low temperatures (strain hardening) to time-dependent plasticity (visco-plasticity) at high temperatures,[30] since the rheological parameters $K(T)$, $n(T)$, and $m(T)$ are continuous functions of temperature. The first parameter is the consistency of the alloy and has units of stress (MPa). The second and third parameters are the strain hardening exponent and strain rate sensitivity. In the current work, all three parameters were taken from Gleeble experiments conducted during the EMPACT project on AA6063 material in the as-cast state.[24,25] The variation of these rheological parameters as a function of temperature is shown in Figure 4. At temperatures below 373 K (100 °C), the mechanical behavior of the alloy is insensitive to strain rate as $m = 0$, but has considerable strain hardening. At temperatures above 673 K (400 °C), strain hardening is negligible since $n = 0$, but the stress response becomes highly dependent on the applied strain rate. At intermediate temperatures (473 K to 673 K; 200 °C to 400 °C), both strain hardening and strain rate effects are present. Equation 3 has been implemented in ABAQUS using the **PLASTIC, RATE =* option with stress-strain curves provided for eight temperatures (293 K, 373 K, 473 K, 573 K, 673 K, and 773 K (20 °C, 100 °C, 200 °C, 300 °C, 400 °C, and 500 °C), $T_{\mathrm{solidus}}$, and $T_{\mathrm{coal}}$) and three strain rates ($10^{-5}$, $10^{-4}$, and $10^{-3}$/s). Additionally, values for the static yield stress were taken from Eq. [3] using a strain rate of $10^{-6}$/s. At temperatures above $T_{\mathrm{coal}}$, the yield stress is assumed to be equal to the yield stress given by Eq. [3] at $T_{\mathrm{coal}}$. Note that ABAQUS uses linear interpolation to determine the location of the yield surface at intermediate temperatures and strain rates.

## IV. RESULTS AND DISCUSSION

### A. *Residual Strain Measurements and FE Model Validation*

Figure 5 shows the temperature profile in the billet cross section predicted by the FE model at the end of the casting process, along with the radial, axial, and hoop stress components after the billet has cooled to room temperature. In Figure 5(a), the liquid pool appears black. As can be seen, the residual stresses are quite high for all three stress components, ranging between –45 and + 105 MPa. Furthermore, the stress distribution does not appear to vary with the cast length except near the ends, an indication that the steady-state casting regime has been reached. In the central part of the billet, the stresses are tensile but become compressive at the surface. These residual stress states develop because of the fast surface cooling rates applied during the casting process, an effect known as "skin-core,"[31] which efficiently cools the surface of the billet. The cold shell then hinders the contraction of the hot core region, leading to large interior tensile stresses (~100 MPa). The skin-core effect has not only been observed in solidification processes, but also during the quenching of heat treatable alloys,[32] and is thought to be one of the origins of crack formation during casting.[6,33]

The residual stress predictions shown in Figure 5 pose great safety issues during sawing, since the energy released by cutting will initially tend to pinch the saw, and may lead to crack initiation when the cutting blade reaches the interior of the billet, under tensile load. These stress predictions can be verified by comparing the simulation results to the results obtained during the ND experiments. In Figure 6, the residual elastic strains predicted by the FE model along the billet radius are compared to the as-measured residual elastic strains. The predicted values were taken from a row of elements at the midpoint along the billet length. The as-measured error bars in the figure are based on the scatter in the measurements, which is a function of the beam path length within the billet. Beginning with the experimental data, the following observations can be made: (1) the center of the billet is in triaxial tension, whereas its surface is in compression in the hoop and axial directions; (2) the radial strain is always positive while the other two components transition from tensile strain near the billet center to compressive strain at the surface; and (3) the radial and hoop elastic strain measurements are almost identical near the billet center, as required due to symmetry considerations. Please note that although the residual elastic strains in the AA6063 billet section were measured in the radial and hoop directions

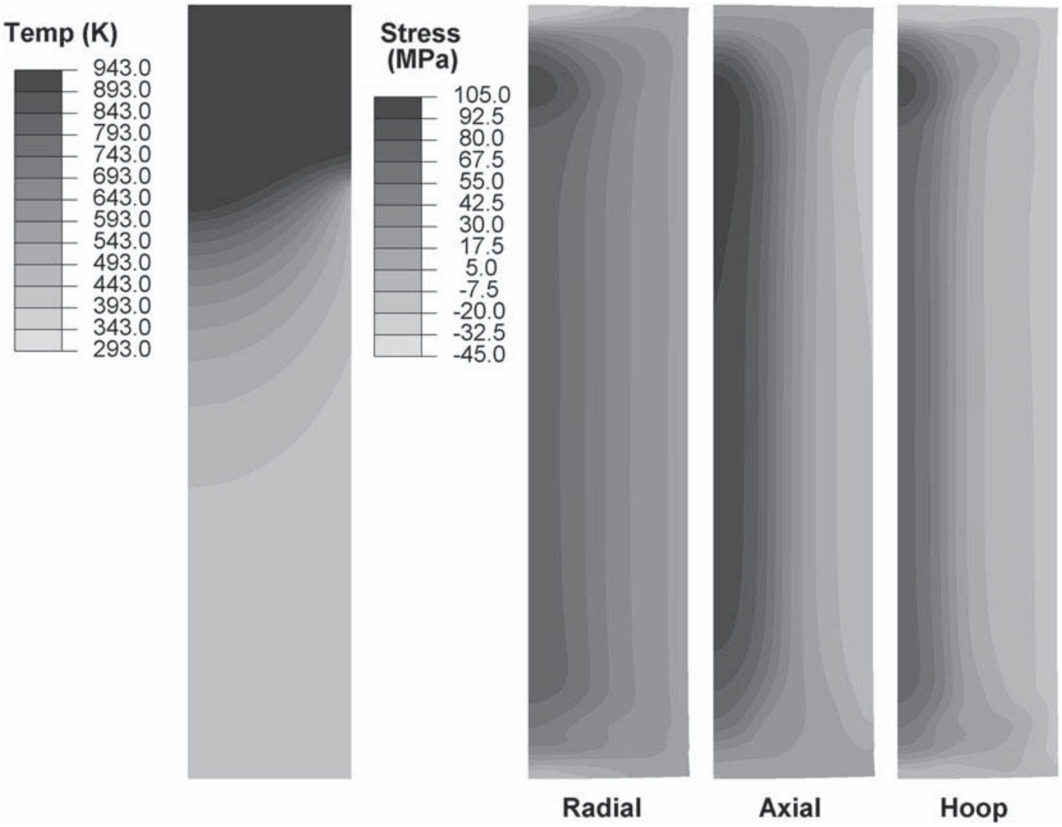

Fig. 5—Temperature field within the billet after 1000 s just prior to the start of cool down, and the stress fields, radial, axial, and hoop, after 4600 s (cool down is complete).

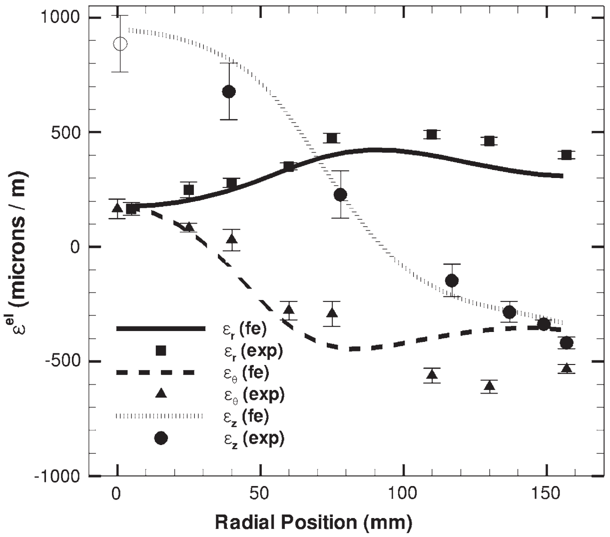

Fig. 6—Comparison between computed and measured residual elastic strain components. The experimental axial strain at the billet center was extrapolated from the other data points and is thus represented by an open circle.

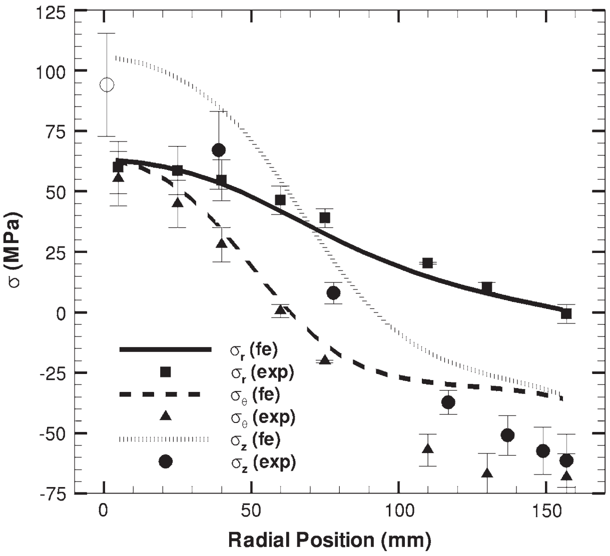

Fig. 7—Comparison between residual stress components computed using the FE model, and those computed using the residual elastic strain measurements in combination with Hooke's Law (ND).

along the entire radius of the billet, the neutron beam was not intense enough to measure the axial strain at the center of the billet. At this location and for the axial strain, the neutron path length of 452 mm was simply too long for measurement in a reasonable amount of time. The quantity provided in Figure 6 was obtained by extrapolating the results of the other axial strain measurements to the centerline of the billet using a polynomial of degree 4. By comparing the residual elastic strain predictions to the as-measured values, it can be seen that the predictions agree quite well with the measured values except for the hoop strain when close to the billet's surface. The experimental-data observations remain valid for the residual elastic strain predictions; it can also be seen that the axial and hoop elastic strains will be equal at the billet surface, as expected due to the geometrical constraints.

In Figure 7, the residual radial, hoop, and axial stresses predicted by the FE model along the billet radius are compared to the stresses components calculated from the ND experiments using Eq. [2]. The error bars on the elastic strain measurement from Figure 6 have been converted to error bars on stress using the elastic constants. Again, the error is rather large for the axial stress. As can be seen in the figure, the agreement between the measured stresses and the FE predictions is quite good for the radial component but weaker for the hoop and axial components, especially at the billet surface. Furthermore, the locations where the predicted axial and hoop stress components change sign are also very close to the measurement values. This transition is important for improving the industrial sawing process, since it is at this point where the billet no longer pinches the saw but rather begins to vibrate due to the release of tensile forces. The observed deviations in hoop and axial stresses near the surface are thought to be caused by nonsymmetric cooling conditions during casting, *i.e.*, variations in the surface roughness or the cooling-water flow rate along the circumference of the billet or by cooling boundary conditions that are not precise enough. A second deviation visible in Figure 7 is that the radial stress should be zero at the billet surface, yet the experimentally determined value is slightly less than zero (–1.65 MPa). This error provides a measure of the precision that can be obtained when making residual elastic strain measurements using neutron measurements.

## B. *Sensitivity Analysis*

As can be seen in Figures 6 and 7, the stress/strain predictions made by the FE model match very well against the experimental results. To the authors' knowledge, this is the first DC casting process model validated with residual stress/strain experimental data along the entire radius from the centerline to the billet's surface. With a validated model of the DC casting process for AA6063 billets, one can perform a sensitivity analysis to determine the relative effect of the various mechanical parameters on residual stress formation. Two model parameters have been investigated: the temperature at the onset of thermal contraction and the plasticity behavior. For the sake of simplicity, the cooling conditions in the primary and secondary zones are kept constant together with the geometry of the billet and the casting speed.

The sensitivity of the model predictions to the start of thermal contraction has been examined by varying the temperature $T_{\text{coal}}$. The results are shown in Figures 8 through 10. For this analysis, the fraction solid for mechanical coalescence was varied from $f_s$ = 0.88 (903 K (630 °C); reference case) to both $f_s$ = 0.95 (865 K (592 °C)) and $f_s$ = 0.80 (914 K (641 °C)). The coalescence fraction solid describes the fraction solid at

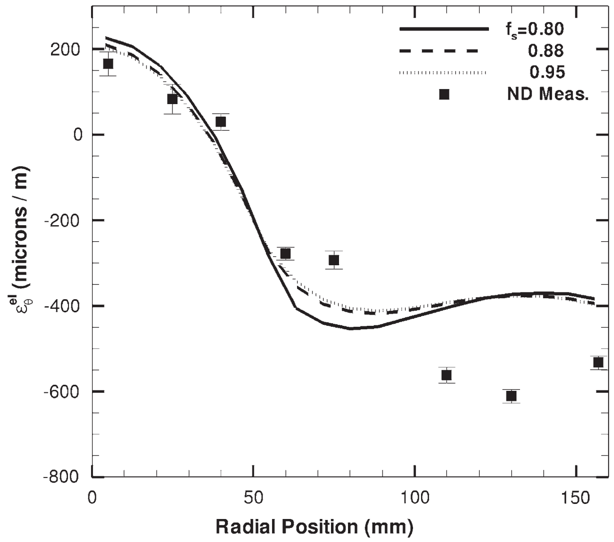

Fig. 8—Effect of coalescence temperature on the hoop elastic strain distribution computed using the FE model. The residual stresses obtained from the ND experiments are also provided.

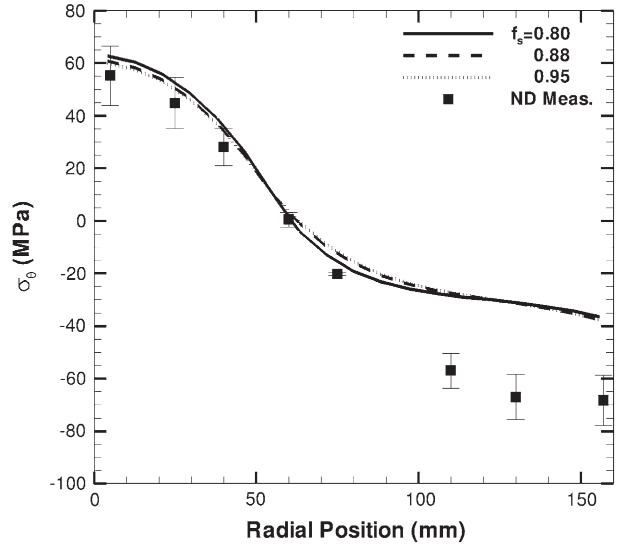

Fig. 9—Effect of coalescence temperature on the hoop stress distribution computed using the FE model. The residual stresses obtained from the ND experiments are also provided.

which the material can sustain long-range tensile stresses. Numerically, the CTE and the Young's modulus are directly affected, as outlined in Section III. The plasticity behavior is also affected since it has been assumed that at temperatures above $T_{\text{coal}}$, the yield stress is assumed to be equal to the yield stress given by Eq. [3] at $T_{\text{coal}}$. The variation of the hoop component of the residual elastic strain is shown in Figure 8 for the three simulations, together with the values measured by ND. As can be seen, the change in coalescence fraction solid has only a moderate effect on the final elastic strains; all three simulations compare well against the experimental data near the centerline of the billet while the comparison is weaker near the billet's surface. The corresponding hoop stresses are plotted in Figure 9, where it appears that varying the coalescence point has a remarkably small influence on this stress component. Note that the predictions of the radial and axial residual stress components for the three different coalescence fraction solids are even more similar than the hoop component.

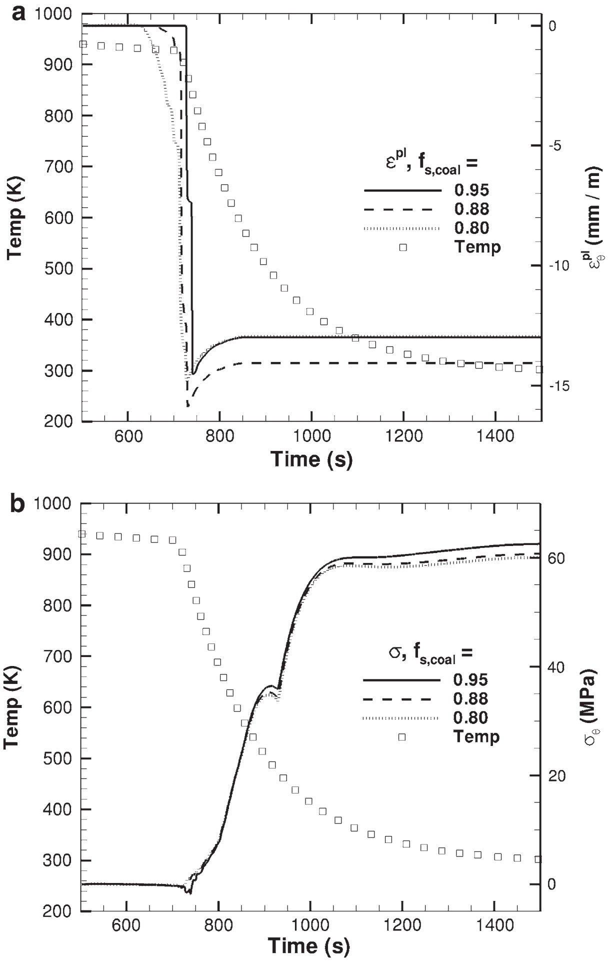

Fig. 10—Simulated (*a*) evolution in temperature and hoop plastic strain and (*b*) evolution in temperature and hoop stress for a point on the billet centerline, midway along its length.

Although as shown in Figures 8 and 9 the coalescence fraction solid has little effect on the final residual stress state, it does have an effect on the accumulation of plastic strain during the casting process. Figure 10 shows the cooling curve for a node located in the steady-state regime (at the centerline of the billet and midway along its height), as well as the evolution in the hoop component of the plastic strain (Figure 10(a)) and the hoop component of stress (Figure 10(b)) at this node. What is most interesting here is that while the stress curves for the three different cases are nearly identical, the plastic strain curves are not. In fact, the largest compressive plastic strain is accumulated for the simulation when $f_{s,\text{coal}} = 0.88$ (–1.4 pct), while the two other cases with $f_{s,\text{coal}} = 0.80$ and 0.95 accumulate

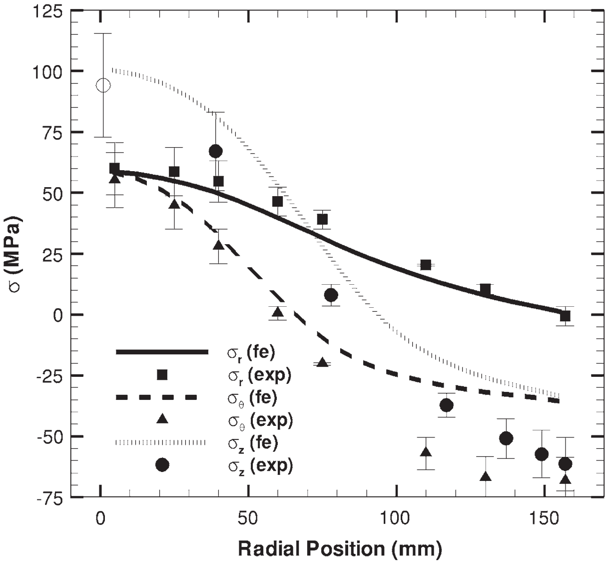

Fig. 11—Comparison between the residual stress predictions computed by the FE model using a pure strain-hardening model and the values obtained from the ND experiments.

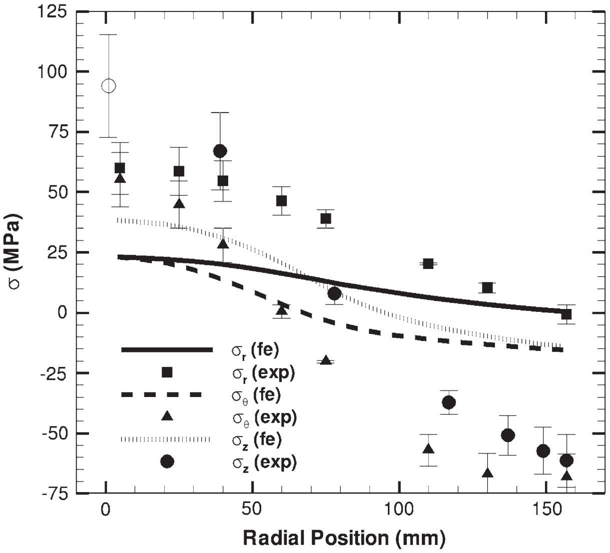

Fig. 12—Comparison between the residual stress predictions computed by the FE model using a pure visco-plastic model and the values obtained from the ND experiments.

approximately 8 pct less plastic strain. The majority of the strain is accumulated at high temperatures, during the initial cooling. This result demonstrates that while the residual stresses are not sensitive to the coalescence point or the temperature at the onset of thermal contraction, this parameter remains important for defects that form during the casting process itself, such as hot tearing, cold cracking, and as-cast porosity.

In order to examine the influence of the plasticity behavior on residual stress predictions, the results from two other simulations have been analyzed. In the first simulation, the strain rate dependency has been removed, resulting in a pure strain hardening model for plasticity behavior. Numerically, only the stress-strain curves from Eq. [3], for the case with a strain rate of $10^{-6}$ $s^{-1}$ at all temperatures, were input into the model. In the second simulation, the strain hardening was eliminated by fixing the strain to 0.001 in Eq. [3], and hence, a pure visco-plastic model is obtained. The computed stress distributions for the pure strain hardening model are presented in Figure 11 together with the measured values. As can be seen, the computed stresses do not differ much from the computational results obtained with the full rheological model using the parameters of Figure 4 and presented in Figure 7.

On the other hand, when strain hardening is eliminated above the yield point, the computed residual stresses are much lower than the measured values, as shown in Figure 12. At the billet center, the three stress components are 3 times lower when compared to the values obtained using the full model or even the strain-hardening model of Figure 11. This result comes from the fact that using a pure visco-plastic model at all temperatures reduces drastically the flow stress of the material during the simulation.

Based on Figures 8 through 12, it is clear that the residual stresses in the as-cast billet are mainly affected by the mechanical properties of the alloy at low temperatures. In other words, using a strain hardening model and ignoring rate dependency at all temperatures is sufficient when computing the as-cast residual stresses. This result is consistent with both the findings of Bru *et al.*,[34] who showed that the residual stresses in welding are mainly affected by the low-temperature mechanical properties, as well as the findings of Dye *et al.*,[35] who examined residual stresses in quenched Ni-based superalloys. In both previous studies, the material investigated was quenched during cooling in order to achieve the desired final mechanical properties. The DC casting process, with spray-water cooling on the sides for heat withdrawal can also be considered as a quenching process. Although the residual stresses are mainly a product of the low-temperature mechanical behavior, the bulk distortions (pull-in, butt curl, *etc.*) that occur due to plastic deformation and thermal contraction will be affected mainly by the high-temperature mechanical behavior including the coalescence point.

## V. CONCLUSIONS

A series of radial, hoop, and axial residual elastic strain values, experimentally measured on an aluminum alloy AA6063 grain-refined cylindrical billet using ND, have been used to validate a thermomechanical that simulates the DC casting process. The corresponding residual stresses indicate that while the billet center is in high tri-axial tension, the billet skin is in bi-axial compression owing to the skin-core effect. These stresses are similar to the stress state encountered in quenching and welding. However, these conclusions might not hold for other aluminum alloys, geometries, or casting recipes especially if hot tears or cold cracks appear.

Using this validated model, the sensitivity of residual stress predictions to input material properties (elastic modulus, CTE, and mechanical behavior) was then investigated. This analysis showed the following.

1. The elimination of strain hardening has a much larger influence on the residual stress predictions as compared to the elimination of the strain rate effects. Hence, it is the alloy's low-temperature mechanical properties that are key for accurate prediction of residual stresses associated with DC casting.
2. The temperature at the onset of thermal contraction has little influence on the final stress distribution within the billet.
3. The temperature at the onset of thermal contraction has a significant effect on the accumulation of plastic strain during the casting process, which will impact the initiation of three common DC casting defects: hot tearing, cold cracking, and as-cast billet distortions.

## ACKNOWLEDGMENTS

The authors express their sincere thanks to C. Jaquerod, Alcan ATI (Valais, Switzerland), for providing the experimental AA6063 billet, and A. Evans, Swiss Spallation Neutron Source, Paul Scherrer Institut (Villigen, Switzerland) for his expertise and assistance with the ND measurements using the POLDI apparatus. One of the authors (AP) also acknowledges the Natural Sciences and Engineering Research Council of Canada for financial assistance.

## REFERENCES

1. J.-M. Drezet: Ph.D. Thesis no. 1509, dir. M. Rappaz, Ecole Polytechnique Federale de Lausanne, Lausanne, 1996, http://library.epfl.ch/theses/?display=detail&nr=1509.
2. J.-M. Drezet and M. Rappaz: *Metall. Mater. Trans. A*, 1996, vol. 27A, pp. 3214–25.
3. B. Hannart, F. Cialti, and R. Schalkwijk: *Light Metals,* A.T. Taberaux, ed., San Francisco, CA, 1994, TMS, Warrendale, PA, 1994, pp. 879–87.
4. H.G. Fjaer and A. Mo: *Metall. Mater. Trans. B*, 1990, vol. 21B, pp. 1049–61.
5. J. Sengupta, S.L. Cockcroft, D.M. Maijer, and A. Larouche: *Mater. Sci. Eng. A*, 2005, vol. 397, pp. 157–77.
6. W. Boender, A. Burghardt, E.P. Van Klaveren, and J. Rabenberg: *Light Metals*, A.T. Taberaux, ed., Charlotte, NC, 2004, TMS, Warrendale, PA, 2004, pp. 679–84.
7. O. Ludwig, J.-M. Drezet, B. Commet, and B. Heinrich: *Model Casting, Welding and Advanced Solidification Processing XI*, C.A. Gandin and M. Bellet, eds., Nice, France, 2006, TMS, Warrendale, PA, 2006, pp. 185–92.
8. W. Droste, J.-M. Drezet, G.-U. Grun, and W. Schneider: in *Continuous Casting*, K. Ehrke and W. Schneider, eds., Wiley-VCH, Frankfurt, 2000, pp. 175–83.
9. W. Droste, G.-U. Grun, W. Schneider, and J.-M. Drezet: *Light Metals,* W. Schneider, ed., Seattle, WA, 2002, TMS, Warrendale, PA, 2002, pp. 703–08.
10. A.B. Phillion, D. Maijer, and S.L. Cockcroft: *Model Casting, Welding and Advanced Solidification Processing XI*, C.A. Gandin and M. Bellet, eds., Opio, France, 2006, TMS, Warrendale, PA, pp. 807–14.
11. K. Escobar, B.B. Gonzalez, J.L. Ortiz, P.N. Nguyen, D. Bowden, J. Foyos, J. Ogren, E.W. Lee, and O.S. Es-Said: *Mater. Sci. Forum*, 2002, vols. 396–402, pp. 1235–40.
12. S. Ganguly, M.E. Fitzpatrick, and L. Edwards: *Mater. Sci. Forum*, 2005, vols. 790–791, pp. 223–28.
13. J. Moriceau: in *Light Metals,* R. Rentsch, ed., TMS, Warrendale, PA, 1975, pp. 119–33.
14. J.S. Robinson, C.E. Truman, S. Hossain, and R. Wimpory: *Mater. Sci. Forum*, 2008, vols. 571–572, pp. 113–18.
15. M.B. Prime: *Appl. Mech. Rev.*, 1999, vol. 52, pp. 75–96.
16. J. Lu: *Handbook of Measurement of Residual Stresses,* The Society for Experimental Mechanics Inc., The Fairmont Press, New York, NY, 1996.
17. L. Bichler, C. Ravindran, and D. Sediako: *Can. Met. Q.*, 2009, vol. 48, pp. 81–90.
18. H. Hao, D.M. Maijer, M.A. Wells, A.B. Phillion, and S.L. Cockcroft: *Metall. Mater. Trans. A*, 2010, vol. 41A, pp. 2067–77.
19. J.-M. Drezet, A. Evans, C. Jaquerod, and A.B. Phillion: *Jim Evans Honorary Symp.*, Seattle, WA, 2010, B. Li, B. Thomas, L. Zhang, F. Doyle, and A. Campbell, eds., TMS, Warrendale, PA, 2010, pp. 43–50.
20. U. Stuhr: *Nucl. Instrum. Methods Phys. Res. A*, 2005, vol. 545, pp. 319–29.
21. U. Stuhr, J. Spitzer, A. Egger, P. Hofer, P. Rasmussen, D. Graf, A. Bollhalder, M. MSchild, G. Bauer, and W. Wagner: *Nucl. Instrum. Methods Phys. Res. A*, 2005, vol. 545, pp. 330–38.
22. J.-M. Drezet, M. Rappaz, G.U. Grun, and M. Gremaud: *Metall. Mater. Trans. A*, 2000, vol. 31A, pp. 1627–34.
23. X. Doré, H. Combeau, and M. Rappaz: *Acta Mater.*, 2000, vol. 48, pp. 3951–62.
24. EMPACT: *European Modelling Programme on Aluminium Casting Technology*, European Union Research Project No. BE-1112, 1996–2000.
25. J.-M. Drezet, B. Commet, H.G. Fjaer, and B. Magnin: *Model Casting, Welding and Advanced Solidification Processing IX*, Aachen, DM, 2000, P.R. Sahm, P.N. Hansen, and J.G. Conley, eds., TMS, Warrendale, PA, 2000, pp. 33–40.
26. A.B. Phillion, S. Thompson, S.L. Cockcroft, and M.A. Wells: *Mater. Sci. Eng. A*, 2008, vol. 497, pp. 388–94.
27. A. Strangeland, A. Mo, and D.G. Eskin: *Metall. Mater. Trans. A*, 2006, vol. 37A, pp. 2219–29.
28. A.B. Phillion, S.L. Cockcroft, and P.D. Lee: *Acta Mater.*, 2008, vol. 56, pp. 4328–38.
29. B. Magnin, L. Maenner, L. Katgerman, and S. Engler: *Mater. Sci. Forum*, 1996, vols. 217–222, pp. 1209–14.
30. W.M. van Haaften, B. Magnin, W.H. Kool, and L. Katgerman: *Metall. Mater. Trans. A*, 2002, vol. 33A, pp. 1971–80.
31. J.-M. Drezet and M. Rappaz: *Proc. 4th Eur. Conf. on Residual Stresses*, S. Denis, ed., Société Francaise de Métallurgie et Matériaux, Cluny, France, 1996, pp. 357–66.
32. F. Heymes, B. Commet, B. Dubost, P. Lassince, P. Lequen, and G.M. Reynaud: *1st Int. Non-Ferrous Processing and Technology Conf.*, St. Louis, MO, 1997, T. Bains, S. Mackenzie, and G.M. Davidson, eds., ASM INTERNATIONAL, Materials Park, OH, 1997, pp. 249–55.
33. M. Lalpoor, D.G. Eskin, and L. Katgerman: *Metall. Mater. Trans. A*, 2009, vol. 40A, pp. 3304–13.
34. D. Bru, J. Devaux, J.M. Bergheau, and D. Pont: *Mathematical Modeling of Weld Phenomena 3*, H. Cerjak, ed., The Institute of Metals, Graz, Austria, 1997, pp. 456–63.
35. D. Dye, K.T. Conlon, and R.C. Reed: *Metall. Mater. Trans. A*, 2004, vol. 35A, pp. 1703–13.